01 Jan 1967

A Plastic Stress Analysis Of Cylindrical Wafers Under Elastically Deformable Compression Plates

Robert L. Davis
Missouri University of Science and Technology, rdavis@mst.edu

J. W. Jackson

R. L. DAVIS

Engineering Mechanics,
University of Missouri,
Rolla, Mo.

J. W. JACKSON

Mechanical Engineering Department,
University of Maryland,
College Park, Md.
Mem. ASME

A Plastic Stress Analysis of Cylindrical Wafers Under Elastically Deformable Compression Plates

This paper represents an analysis of the pressure distribution occurring in axially loaded cylindrical wafers with, and without, elastic radial constraints. The purpose of this report is to demonstrate the resulting stress patterns that occur in short compression specimens frequently used in determining material properties, and in the opposed-anvil, or Bridgman-type, high-pressure cells. The influence of radial constraints, material strain hardening, wafer diameter-to-height ratio, anvil or plate deflection, and the wafer-anvil interface friction on the resulting stress distributions have been examined. The integrated normal stress distribution across the specimen surface has been verified experimentally via numerous tests in which each of the subject parameters listed above was varied.

Introduction

THE problem of specific interest here is the study of the radial and axial pressure gradients existing in a circular specimen situated between a pair of initially parallel compression plates, called anvils. Other investigators [1, 2, 3, 4][1] have analytically described the resulting phenomenon by employing certain simplifying assumptions in their analyses in order to reduce the problem to a more tractable form. Since these assumptions are not entirely defensible, and the end results have not been verified, the justification for a more extensive analysis is apparent.

Considerable effort has been expended to determine experimentally the stress state in nonmetallic specimens, and this merits a brief discussion. The resistance change in manganin wire, as a function of pressure, has served as a basis for an experimental evaluation of pressure gradients in circular wafers of silver chloride, reference [5]. The manganin wire was formed into a hoop of constant radius in accordance with the assumed axial symmetry. This technique prevented any axial variations from influencing measurements of the radial gradients, and the converse is true for axial measurements. In reference [6], the pressure-induced phase change of bismuth wire was employed to obtain specific load-pressure data. The authors of this reference placed bismuth wires in both axial and radial positions in an effort to isolate and define the gradients occurring in these two directions. The results reported in reference [5] indicate that

pressure is lowest at the wafer center and increases linearly with increase in radial position. Reference [6] suggests that this result is possible, but would be largely dependent on the diameter to thickness ratio (D/H) of the wafer. The authors of reference [7] have used the techniques described in reference [6] with the result that the pressure is always highest at the center of pyrophyllite, talc, and boron nitride wafers. This reference also mentions the existence of axial variations in confined wafers of variable D/H ratios, and points out the influence of the anvil-wafer friction on this variation. These conclusions are definitely compatible with the results of this report. Since the actual pressure mechanism which generates these phase and resistance changes has not been conclusively described, most experimenters have been compelled to define pressure in terms of total compressive load, divided by wafer area. This is actually a measure of the average axial normal stress and would supposedly exist only at the mid-merdian plane by virtue of the presence of shearing stress on the deflected wafer surface. Pressure is usually defined as the average of the orthogonal stress state existing at a point and will be referred to as such in this report. Unksov, reference [3], has presented experimental evidence of the contact stresses for lead and metallic specimens and has reviewed the results of several other experimenters. Also of interest in this reference is the comparative discussion of the theoretical analysis for the assumption of plane strain (as suggested by Prandtl) and the experimental results for circular specimens. The two results are quantitatively the same. The purpose of discussing these reports is to point out the difficulty to be encountered by experimenters in attempting to isolate, and predict, the influence of changes in all of the probable parameters. Chief among the parameters needed to be studied are: diameter-to-thickness ratio; wafer material properties (strain hardening and yield

---

[1] Numbers in brackets designate References at end of paper.

Nomenclature

a_1, a_2, a_3 = displacement coefficients	$2h_c$ = deformed wafer height measured along the wafer axis	which the longitudinal coordinate is directed along the wafer axis
b = slope of plastic stress-strain curve	P_c = radial restraining pressure exerted on the wafer at the mid-meridian plane by the containing ring	R_0 = initial wafer radius
F = applied force transmitted to the wafer from the compression anvils		R_c, R_t = deformed wafer radius measured at the mid-meridian and top surfaces, respectively
f = coefficient of friction at wafer-anvil interface	r, θ, z = radial, circumferential, and longitudinal coordinates, respectively, of cylindrical coordinate system in	R_a = radial position, measured on wafer-anvil interface,
G = modulus of rigidity of anvil material		
$2h_0$ = initial wafer height		*(Continued on next page)*

strength); anvil-wafer friction effect; anvil deflection; and influence of radial constraints.

This paper is a condensed version of a more elaborate report (reference [8]) made available to Pressure Science, Inc., Beltsville, Md., and limited copies may be obtained from the authors.

Stress Analysis

The discussion of a stress analysis involving the compression of wafers in an opposed-anvil apparatus necessitates an agreement on the terminology to be employed. The wafer is initially in the form of a short, right circular cylinder and is located between an identical pair of parallel plates, called anvils. As these anvils are brought close together, a compressive force is generated on, and in a direction perpendicular to, the parallel surfaces of the wafer. This loading causes the wafer to expand in the radial direction; however, the original cylindrical shape of the wafer is not necessarily maintained. The expanding wafer is retarded at the wafer-anvil interfaces by the inherent shearing action and consequently deforms into a barrel shape (barreling). If the compression plates are nonrigid, then they too will undergo a certain deformation pattern with change in load. The assumed elastic behavior of the anvils requires that they return to their initial parallel position upon unloading. However, the wafer is allowed to flow plastically and will, in general, be permanently distorted. Fig. 1 is a qualitative view of the wafer in the deformed state. If the wafer maintains its cylindrical shape during expansion, then the single radial coordinate r can be used to describe the process. The possession of axial symmetry eliminates the variation of any parameters with the circumference coordinate θ. In the more general case, variations are occurring in the axial direction z and must be accounted for. The center of the wafer is shown to be the thinnest section; however, this is not a necessary assumption in that the analysis will dictate the required direction of curvature.

The admittance of an elastic containing ring around the wafer retards its radial motion and significantly raises the stress level within the wafer. This, and other techniques, has been responsible for the generation of pressures of the magnitude required for bismuth phase changes as discussed earlier. In this analysis, the containing ring acts only on the wafer, hence the entire compressive force of the anvils is directed through the wafer.

In order to effectively demonstrate the influence of the parameters under study, a single wafer material, called the primary material, was utilized in those tests where the material constants were not variable. Additional experiments were conducted with different wafer materials, called the secondary materials, to evaluate the material effect. The selection of the primary wafer material was based on the following factors: (1) the wafer material must strain harden in an essentially linear fashion (this is required for consistency with the Ludwik equation, discussed later); (2) have high ductility; (3) possess a high degree of strain hardening; and (4) be nearly incompressible as required in equation (1). The secondary wafer material must have properties

LEGEND:
INITIAL STATE ———
LOADED CONDITION – – – –

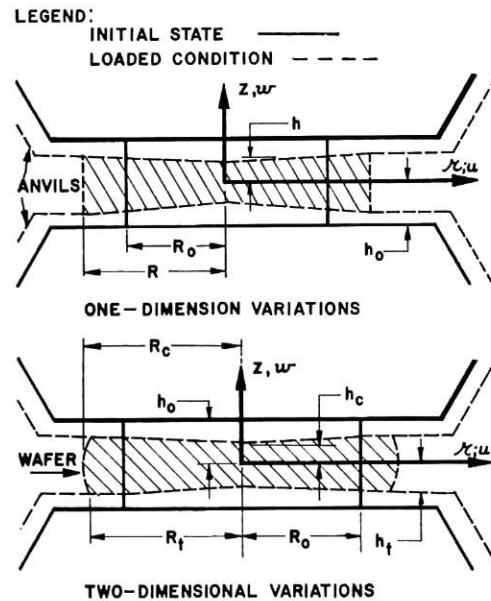**ONE–DIMENSION VARIATIONS**

TWO–DIMENSIONAL VARIATIONS

Fig. 1 Postulated wafer profile for one and two-dimensional analysis

that are compatible with the latter and should otherwise reflect changes only in those parameters under study. The above reasoning led to the selection of annealed 303 stainless steel for the primary material, and 2S aluminum, 6061 aluminum, and Armco iron for the secondary materials.

The approach to be taken here is to first describe the system of equations to be used, present the method of solution, and then show the resulting stress distributions for each of the situations under study.

(A) Formulation of Governing Equations. The system of equations to be developed here is patterned from those given by Hoffman and Sachs in reference [7] for a rigid-plastic material. It has been stated in reference [8], that for predominantly plastic strains, such as occur in most metal-forming operations, the material may be considered incompressible. The condition of volume constancy (for small total strains) may be written as

$$\epsilon_r + \epsilon_\theta + \epsilon_z = 0 \qquad (1)$$

where ϵ_r, ϵ_θ, and ϵ_z are the normal engineering strains acting in the radial, tangential, and axial directions, respectively. Since the wafer is axially symmetric, the strains are defined in terms of the displacements as

$$\epsilon_r = \frac{\partial u}{\partial r}, \qquad \epsilon_\theta = \frac{u}{r}, \qquad \epsilon_z = \frac{\partial \omega}{\partial z}$$

$$\gamma_{rz} = \frac{\partial u}{\partial z} + \frac{\partial \omega}{\partial r} \qquad (2)$$

———— Nomenclature————

where shear yielding commences

u, w = radial and axial wafer displacements, respectively

$\alpha_1, \beta_1, \gamma_1$ = selected coefficients containing z-coordinate variations

$\beta_1{}', \gamma_1{}'$ = derivatives of above coefficients with respect to z-coordinate

$\epsilon_r, \epsilon_\theta, \epsilon_z$ = radial, circumferential, and longitudinal wafer strains, respectively

$\bar{\epsilon}$ = effective strain

$\epsilon_{\theta c}$ = circumferential strain occurring at outer surface of containing ring

γ_{rz} = wafer shearing strain

$\sigma_r, \sigma_\theta, \sigma_z$ = radial, circumferential, and longitudinal normal stresses, respectively

$\bar{\sigma}$ = effective stress

τ_{rz} = wafer shearing stress

σ_0, τ_0 = normal and shear yield stresses, respectively

$\nabla_1, \nabla_2, \nabla_3$ = operators (equivalent to standard Laplacian operator except for sign differences)

∇ = deformed wafer center line deflection

ψ = displacement function

δ = radial wafer deflection measured at the mid-meridian plane

ν = Poisson's ratio for anvil material

where u and ω are the radial and axial displacements, respectively, and γ_{rz} is the only nonvanishing shearing strain.

Utilizing the Hencky Deformation theory, the resulting stress-strain relations, valid in the plastic domain, can be written as

$$\frac{2\sigma_\theta - \sigma_r - \sigma_z}{2\sigma_r - \sigma_\theta - \sigma_z} = \frac{\epsilon_\theta}{\epsilon_r}$$

$$\frac{2\sigma_z - \sigma_r - \sigma_\theta}{2\sigma_r - \sigma_\theta - \sigma_z} = \frac{\epsilon_z}{\epsilon_r}$$
(3)

$$\frac{6\tau_{rz}}{2\sigma_r - \sigma_\theta - \sigma_z} = \frac{\gamma_{rz}}{\epsilon_r}$$
(4)

where σ_r, σ_θ, and σ_z are the normal stresses acting in the radial, tangential, and axial direction, respectively, and τ_{rz} is the only nonvanishing component of shearing stress. The first two of these equations are not independent, in that they reduce to a statement of volume constancy when combined. Thus only two equations are obtained from the deformation theory.

The Hencky theory furnishes results identical with those of Saint Venant's flow theory under two conditions: (a) that the principal axes of stress and strain for a particle do not rotate with respect to the particle during the process of straining; and (b) that the straining is "proportional," that is, the strain increments are proportional to the total strains. These conditions are essentially satisfied for small finite strains (less than 20–30 percent) if there is no shear on any of the wafer surfaces, and the wafer maintains its cylindrical shape during loading. The same is approximately true for small amounts of shear at the wafer-anvil interfaces. This imposed, yet defensible, restriction on the nature and degree of straining within the wafer has led to the use of classical, or engineering type, strains in lieu of the more appropriate true strain increments.

The von Mises yield criteria can be used to predict the incipience of plastic yielding in ductile metals. This theory is independent of the hydrostatic component of stress and requires the knowledge of a single material constant, the "effective stress" in uniaxial state of stress, in order to predict the behavior under any given combination of principal stresses. The applicable yield criteria is written as

$$(\sigma_r - \sigma_\theta)^2 + (\sigma_\theta - \sigma_z)^2 + (\sigma_z - \sigma_r)^2 + 6\tau_{rz}^2 = 2\bar{\sigma}^2 \quad (5)$$

where $\bar{\sigma}$ is the effective stress taken from a uniaxial compression test. The effective stress is assumed to be linear with respect to the effective strain as called for in the selection of the wafer material. Thus, the linear form of the Ludwik equation, reference [11], becomes

$$\bar{\sigma} = \sigma_0 + b\bar{\epsilon} \quad (6)$$

where σ_0 is the yield stress at the onset of plastic strain, b is the slope, and $\bar{\epsilon}$ is the effective strain in the plastic region. An inherent implication here is that the wafer material is rigid until the incipience of plastic strain, and then strains in a linear fashion. Unksov discusses, in reference [3], the occurrence of regions in the deformed wafer that remain essentially elastic during the loading process. However, for wafer diameter-to-height (D/H) ratios greater than unity (which is the situation in this report), the volume of material contained in these elastic regions is very small, and continues to decrease with increase in the D/H ratio. Thus the assumption that the wafer material is fully plastic is justified. The effective strain for a material that is rigid up to yield is given in reference [12] as

$$\bar{\epsilon} = \frac{\sqrt{2}}{3}\left[(\epsilon_r - \epsilon_\theta)^2 + (\epsilon_\theta - \epsilon_z)^2 \right.$$

$$\left. + (\epsilon_z - \epsilon_r)^2 + \frac{3}{2}\gamma_{rz}^2 \right]^{1/2} \quad (7)$$

The von Mises yield theory is thus a combination of equations (5), (6), and (7).

The two equilibrium equations for cylindrical coordinates are easily developed from the stress state acting on a differential volume element taken from the wafer in the loaded state. They are

$$\frac{\partial \sigma_r}{\partial r} + \frac{\sigma_r - \sigma_\theta}{r} + \frac{\partial \tau_{rz}}{\partial z} = 0 \quad (8)$$

$$\frac{\partial \tau_{rz}}{\partial r} + \frac{\partial \sigma_z}{\partial z} + \frac{\tau_{rz}}{r} = 0 \quad (9)$$

The foregoing system of equations, combined with the appropriate boundary conditions, are sufficient for a complete determination of the displacements, strains, and stresses occurring in the plastically deformed wafer.

(B) Method of Solution. If the displacements u and w are defined in terms of a displacement function ψ as

$$u = \frac{1}{r}\frac{\partial \psi}{\partial z}, \qquad w = -\frac{1}{r}\frac{\partial \psi}{\partial r} \quad (10)$$

then the volume constancy equation (1) is satisfied identically. The utility of a displacement function becomes apparent when it is realized that the previous system of equations can be reduced to a single equation, involving only the displacement function and the characteristic wafer material properties. Once the appropriate displacement function is determined, or approximated, the strains and displacements can be found directly.

The formulation of this equation is completed by appropriately combining the plasticity equations in the following chronological order: equations (3) and (4), flow laws; (5), yield criterion; (6) material strain hardening; (7) effective strain; (8) and (9), equilibrium equations; and finally equations (10), definition of the displacement function ψ. The manipulation is lengthy, but direct, and eventually leads to the desired result, equation (11).

$$\frac{\bar{\sigma}}{\bar{\epsilon}}\nabla_1^4\psi + \nabla_3^2\psi\nabla_2^2\left(\frac{\bar{\sigma}}{\bar{\epsilon}}\right) + \frac{2}{r}\frac{\partial}{\partial z}\left(\frac{\partial \psi}{\partial r} - \frac{2\psi}{r}\right)\frac{\partial}{\partial z}\left(\frac{\bar{\sigma}}{\bar{\epsilon}}\right)$$

$$+ 2\frac{\partial}{\partial z}\left(2\frac{\partial \psi}{\partial r} - \frac{\psi}{r}\right)\frac{\partial^2}{\partial r \partial z}\left(\frac{\bar{\sigma}}{\bar{\epsilon}}\right) = 0 \quad (11)$$

where the operators ∇_1, ∇_2, and ∇_3 are equivalent to the standard Laplacian operator, except for the indicated sign changes.

$$\nabla_1^2 = \frac{\partial^2}{\partial r^2} - \frac{1}{r}\frac{\partial}{\partial r} + \frac{\partial^2}{\partial z^2}$$

$$\nabla_2^2 = \frac{\partial^2}{\partial r^2} + \frac{1}{r}\frac{\partial}{\partial r} - \frac{\partial^2}{\partial z^2}$$

$$\nabla_3^2 = \frac{\partial^2}{\partial r^2} - \frac{1}{r}\frac{\partial}{\partial r} - \frac{\partial^2}{\partial z^2}$$

Equation (11) represents the governing equation for determining the displacement function ψ. The prospect of obtaining an exact solution of (11) for an arbitrary material is improbable at this point, and a numerical solution would likewise be difficult by virtue of the mixed boundary conditions. If the compression specimen were constructed from a linearly plastic Newtonian material (i.e., the ratio of effective stress and effective strain is constant), only the first term in equation (11) remains, and the solution to this simplified differential equation is presented, with discussion, in reference [10]. An alternate approach, and the one to be used here, is to select a displacement function ψ that approximately satisfies the governing equation (11) and will yield a prescribed displacement pattern which is consistent with the observed shape of the loaded wafer.

1 Two-Dimensional Wafer Profile—With Shear. The assumed profile of the water in the loaded state has been portrayed in Fig. 1 and leads to the following trial for the displacement function ψ,

$$\psi = a_1 r^4 z + a_2 r^2 z^3 + a_3 r^2 z \quad (12)$$

where a_1, a_2, and a_3 are constants and will be referred to as displacement coefficients. Using this function with equations (10), the displacements become

$$u = a_1 r^3 + (3a_2 z^2 + a_3) r \quad (13)$$

$$\omega = -2z(2a_1 r^2 + a_2 z^2 + a_3) \quad (14)$$

An examination of (13) indicates that the wafer can barrel in a parabolic fashion, having symmetry with respect to the mid-meridian wafer plane. Equation (14) shows that the wafer-anvil interface can likewise be deformed into a parabola; the line of symmetry being coincident with the wafer axis. Thus, the trial form of the displacement function ψ, as given in equation (12), does describe a wafer deformation pattern that is consistent with that shown in Fig. 1.

By taking the appropriate derivatives of the displacements, the strains are found to be

$$\epsilon_r = 3a_1 r^2 + 3a_2 z^2 + a_3 \quad (15)$$

$$\epsilon_\theta = a_1 r^2 + 3a_2 z^2 + a_3 \quad (16)$$

$$\epsilon_z = -4a_1 r^2 - 6a_2 z^2 - 2a_3 \quad (17)$$

$$\gamma_{rz} = 2rz(3a_2 - 4a_1) \quad (18)$$

In order to evaluate the accuracy of the chosen function ψ, equation (12) is substituted, together with a combination of equations (6), (7), (15), (16), (17), and (18), into the governing equation (11). Equation (12) satisfies the first term of (11) identically at all points and is in agreement with the remaining terms of (11) if attention is restricted to the wafer axis and mid-meridian plane. A study of the remaining points of the wafer, using typical values of the displacement coefficients, shows that the largest discrepancy involved in satisfying equation (11) is of the order of one-tenth the effective strain squared. This agreement, both in satisfying the governing equation (11) and in describing the resulting deformation pattern, provides strong endorsement of the use of equation (12) as an excellent choice of the displacement function. Additional satisfaction will be acquired when the end results of this analysis are compared with the results of the experimental program.

When equations (15) through (18) are combined with (7), the effective strain becomes

$$\bar{\epsilon} = (\alpha_1 r^4 + \beta_1 r^2 + \gamma_1)^{1/2} \quad (19)$$

where

$$\alpha_1 = \frac{52}{3} a_1{}^2, \qquad \gamma_1 = 4(3a_2 z^2 + a_3)^2$$

$$\beta_1 = \frac{4}{3} [(12a_1 a_2 + 9a_2{}^2 + 16a_1{}^2)z^2 + 12a_1 a_3] \quad (20)$$

The first derivative with respect to z of the foregoing coefficients will be required later and are documented here as

$$\beta_1{}' = \frac{8}{3} (12a_1 a_2 + 9a_2{}^2 + 16a_1{}^2)z$$

$$\gamma_1{}' = 48a_2(3a_2 z^2 + a_3)z \quad (21)$$

With the strains now known, the equilibrium equation (8), which can be written with the aid of equations (3), (4), (5), (6), and (7), as a function of the radial stress alone, can be integrated to give the result shown in (22). The integration is lengthy, but can be accomplished with the formulas appearing in a short table of integrals. The constant of integration is assessed by requiring that the radial stress be equal to the containing pressure P_1 at the external wafer surface. If the containing ring is absent, P_1 vanishes. The remaining stresses are easily found from the use of equations previously discussed. The tangential and axial normal stresses are given in (23) and (24), respectively, and equation (25) is the shearing stress.

$$\sigma_r = \frac{\sigma_0}{3\sqrt{\alpha_1}} (2a_1 - 3a_2)$$
$$\times Ln\left\{\frac{2\alpha_1 r^2 + \beta_1 + 2\sqrt{\alpha_1}[\alpha_1 r^4 + \beta_1 r^2 + \gamma_1]^{1/2}}{2\alpha_1 R^2 + \beta_1 + 2\sqrt{\alpha_1}[\alpha_1 R^4 + \beta_1 R^2 + \gamma_1]^{1/2}}\right\}$$
$$+ \frac{\sigma_0 z(3a_2 - 4a_1)}{3(\beta_1{}^2 - 4\alpha_1\gamma_1)}\left\{\frac{(\beta_1\beta_1{}' - 2\alpha_1\gamma_1{}')r^2 - (\beta_1\gamma_1{}' - 2\gamma_1\beta_1{}')}{[\alpha_1 r^4 + \beta_1 r^2 + \gamma_1]^{1/2}}\right.$$
$$\left. - \frac{(\beta_1\beta_1{}' - 2\alpha_1\gamma')R^2 - (\beta_1\gamma_1{}' - 2\gamma_1\beta_1{}')}{[\alpha_1 R^4 + \beta_1 R^2 + \gamma_1]^{1/2}}\right\}$$
$$+ \frac{b}{3}(2a_1 - 3a_2)(r^2 - R^2) - P_1 \quad (22)$$

$$\sigma_\theta = \frac{\sigma_0}{3\sqrt{\alpha_1}} (2a_1 - 3a_2)$$
$$\times Ln\left\{\frac{2\alpha_1{}^2 r^2 + \beta_1 + 2\sqrt{\alpha_1}[\alpha_1 r^4 + \beta_1 r^2 + \gamma_1]^{1/2}}{2\alpha_1 R^2 + \beta_1 + 2\sqrt{\alpha_1}[\alpha_1 R^4 + \beta_1 R^2 + \gamma_1]^{1/2}}\right\}$$
$$+ \frac{\sigma_0 z(3a_2 - 4a_1)}{3(\beta_1{}^2 - 4\alpha_1\gamma_1)}\left\{\frac{(\beta_1\beta_1{}' - 2\alpha_1\gamma_1{}')r^2 - (\beta_1\gamma_1{}' - 2\gamma_1\beta_1{}')}{[\alpha_1 r^4 + \beta_1 r^2 + \gamma_1]^{1/2}}\right.$$
$$\left. - \frac{(\beta_1\beta_1{}' - 2\alpha_1\gamma_1{}')R^2 - (\beta_1\gamma_1{}' - 2\gamma_1\beta_1{}')}{[\alpha_1 R^4 + \beta_1 R^2 + \gamma_1]^{1/2}}\right\}$$
$$- \frac{4}{3} a_1\sigma_0\left\{\frac{r^2}{[\alpha_1 r^4 + \beta_1 r^2 + \gamma_1]^{1/2}}\right\}$$
$$- \frac{2}{3} a_1 b(r^2 + R^2) - a_2 b(r^2 - R^2) - P_1 \quad (23)$$

$$\sigma_z = \frac{\sigma_0}{3\sqrt{\alpha_1}} (2a_1 - 3a_2)$$
$$\times Ln\left\{\frac{2\alpha_1 r^2 + \beta_1 + 2\sqrt{\alpha_1}[\alpha_1 r^4 + \beta_1 r^2 + \gamma_1]^{1/2}}{2\alpha_1 R^2 + \beta_1 + 2\sqrt{\alpha_1}[\alpha_1 R^4 + \beta_1 R^2 + \gamma_1]^{1/2}}\right\}$$
$$+ \frac{\sigma_0 z(3a_2 - 4a_1)}{3(\beta_1{}^2 - 4\alpha_1\gamma_1)}\left\{\frac{(\beta_1\beta_1{}' - 2\alpha_1\gamma_1{}')r^2 - (\beta_1\gamma_1{}' - 2\gamma_1\beta_1{}')}{[\alpha_1 r^4 + \beta_1 r^2 + \gamma_1]^{1/2}}\right.$$
$$\left. - \frac{(\beta_1\beta_1{}' - 2\alpha_1\gamma_1{}')R^2 - (\beta_1\gamma_1{}' - 2\gamma_1\beta_1{}')}{[\alpha_1 R^4 + \beta_1 R^2 + \gamma_1]^{1/2}}\right\}$$
$$- \frac{2\sigma_0}{3}\left\{\frac{7a_1 r^2 + 9a_2 z^2 + 3a_3}{[\alpha_1 r^4 + \beta_1 r^2 + \gamma_1]^{1/2}}\right\} - \frac{2}{3} a_1 b(6r^2 + R^2)$$
$$- a_2 b(r^2 - R^2) - 6a_2 bz^2 - 2a_3 b - P_1 \quad (24)$$

$$\tau_{rz} = \frac{2}{3} b(3a_2 - 4a_1)rz$$
$$+ \frac{2}{3} \sigma_0 (3a_2 - 4a_1)\left\{\frac{rz}{[\alpha_1 r^4 + \beta_1 r^2 + \gamma_1]^{1/2}}\right\} \quad (25)$$

The foregoing three normal stress equations represent the orthogonal stress state existing at any point in the wafer, and are based on the assumptions of low shear stress, elastic deflection of the anvil and containing ring, linear strain hardening and incompressibility of the wafer material, and wafer diameter-to-height ratios greater than unity. As shown in the next section, the component parts of the experimental apparatus are selected to be compatible with these restrictions. The mean stress or pressure distribution across the diameter of the wafer may be obtained by taking the average of (22), (23), and (24). The area under the axial normal stress σ_z curve, evaluated at

the mid-meridian wafer plane, ($z^* = 0$) corresponds to the applied force transmitted to the wafer from the anvils. The mid-meridian is selected, since at any other plane the wafer is distorted, and is under the influence of shearing stresses, which can support a portion of the applied load. In integral form, the applied force is expressed as

$$F = 2\pi \int_0^{R_c} (\sigma_z)_{z=0} r\, dr \qquad (26)$$

where R_c is the maximum wafer radius in the mid-meridian plane. Substituting equation (24) into (26), and performing the indicated integration, the results shown in equation (27) are obtained. The subscript "c" appearing in subsequent equations indicates that the quantity in question has been evaluated at a radius of magnitude R_c.

$$F = \frac{2\sigma_0\pi}{3\sqrt{\alpha_c}} (2a_1 - 3a_2) \left\{ \frac{2\alpha_c R_c{}^2 + \beta_c}{4\alpha_c} [Ln(2\alpha_c R_c{}^2 + \beta_c) - 1] \right.$$
$$\left. - \frac{\beta_c}{4\alpha_c} [Ln(\beta_c) - 1] - \frac{1}{2} R_c{}^2 \ln(2\alpha_c R_c{}^2 + \beta_c) \right\}$$
$$- \frac{1}{2}(4a_1 + a_2)\pi b R_c{}^4 - \frac{3}{4}\pi\sigma_0$$
$$\times \left\{ 7a_1 \left[\frac{1}{2\alpha_c}(\alpha_c R_c{}^4 + \beta_c R_c{}^2 + \gamma_c)^{1/2} \right. \right.$$
$$- \frac{1}{4}\beta_c \alpha_c{}^{-3/2} \ln \left\{ \frac{\beta_c}{2\sqrt{\alpha_c}} + \sqrt{\alpha_c}\, R_c{}^2 \right.$$
$$\left. + (\alpha_c R_c{}^4 + \beta_c R_c{}^2 + \gamma_c)^{1/2} \right\} - \frac{\sqrt{\gamma_1}}{2\alpha_c}$$
$$\left. + \frac{1}{4}\beta_c\alpha_c{}^{-3/2} \ln\left(\frac{\beta_c}{2\sqrt{\alpha_c}} + \sqrt{\gamma_c} \right) \right]$$
$$+ 3a_3 \left[\frac{1}{2\sqrt{\alpha_c}} \ln\left\{ \frac{\beta_c}{2\sqrt{\alpha_c}} + \sqrt{\alpha_c}\, R_c{}^2 \right. \right.$$
$$\left. + (\alpha_c R_c{}^4 + \beta_c R_c{}^2 + \gamma_c)^{1/2} \right\}$$
$$\left. \left. - \frac{1}{2\sqrt{\alpha_c}} \ln\left(\frac{\beta_c}{2\sqrt{\alpha_c}} + \sqrt{\gamma_c} \right) \right] \right\}$$
$$- \pi \left(\frac{2}{3} a_1 b R_c{}^2 - a_2 b R_c{}^2 + 2a_3 b + P_c \right) R_c{}^2 \quad (27)$$

The resulting displacements (and hence strains, stresses, etc.) in a compressed wafer at any specific axial load can be determined from equations (13) and (14) providing the displacement coefficients a_1, a_2, a_3 and the current wafer dimensions R_c and h_c are known. These unknown quantities can be evaluated by imposing five independent conditions that adequately describe the effects of the physical constraints applicable to the compression of radially confined wafers.

The first boundary condition pertains to the radial deformation at the mid-meridian wafer plane. This condition requires that at

$$r = R_c, \qquad z = 0; \qquad u = R_c - R_0 \qquad (28)$$

where R_0 is the initial wafer radius. A combination of (13) and (28) gives

$$a_1 = \left(\frac{R_c - R_0}{R_c} - a_3 \right) \bigg/ R_c{}^2 \qquad (29)$$

The second condition relates the radial wafer deflection to the constraining pressure. If δ is the radial deflection at the mid-meridian plane, then

$$\delta = R_c - R_0 = (5.32 \times 10^{-8})P_c \qquad (30)$$

where P_c is the restraining pressure exerted on the wafer, at $z = 0$, by the containing ring. The numerical factor appearing in (30) is obtained from an application of the Lame equation for the elastic deformation of a thick-wall cylinder and radial wedges. These equations can also be used to describe the amount of tangential strain $\epsilon_{\theta c}$ occurring at the outer surface of the containing ring, due to the influence of the internal pressure P_c. This is one of the strains monitored in the experimental program. The relation found for the ring used in this program is

$$\epsilon_{\theta c} = (3.02 \times 10^{-9})P_c \qquad (31)$$

A more detailed description of the containing ring and its use is given in a later section. Using equations (13) and (30), the mid-meridian constraint pressure becomes

$$P_c = \left(\frac{R_c}{5.32 \times 10^{-8}} \right) [a_1 R_c{}^2 + a_3] \qquad (32)$$

In the absence of a constraining ring, P_c is zero. If the total axial deflection along the wafer axis is defined as Δ, the third boundary condition becomes

$$r = 0, \qquad z = h_c; \qquad \omega = -\Delta/2 \qquad (33)$$

where h_c is one-half the wafer height, measured along its axis, at any given load. Substituting the conditions of (33) into (14) gives

$$a_3 = \frac{\Delta}{2(2h_0 - \Delta)} - \frac{a_2}{4}(2h_0 - \Delta)^2 \qquad (34)$$

where $2h_0$ is the initial wafer height.

The total amount of shear stress existing on the wafer-anvil interface is considered to be directly proportional to the magnitude of the normal stress acting on this same surface (Coulomb law of friction). The coefficients of friction for various materials, under a pressure of 25 Kb, have been documented in reference [13]. The manner in which these experiments were conducted requires that the integrated effects of the normal and shear stresses be related as follows:

$$\int_0^{R_t} (\tau_{rz})_{z=h_c} r\, dr = f \int_0^{R_t} (\sigma_z)_{z=h_c} r\, dr \qquad (35)$$

where R_t is the external radius, evaluated at the top surface of the loaded wafer. If the shear stress τ_{rz} exceeds the shear strength τ_0 of the wafer material, then equation (35) must be written in the form

$$\int_0^{R_a} (\tau_{rz})_{z=h_c} r\, dr + \int_{R_a}^{R_t} \tau_0 r\, dr = f \int_0^{R_t} (\sigma_z)_{z=h_c} r\, dr \quad (36)$$

where R_a is the radial position where τ_{rz} becomes equivalent to τ_0. The value of τ_0 is considered to be one half of the effective stress $\bar{\sigma}$ at any given stage of strain.

The limits of integration are taken as shown since the shear stress is zero at the wafer axis and increases with increase in radial position. The computer program used in solving this problem first calculates the shear stress at the top surface of the wafer and then runs a comparison check between τ_{rz} and τ_0 at ten equally spaced intervals across the wafer. If τ_{rz} is less than τ_0 at all radial positions, then R_a is set equal to R_t and equation (36) reduces to (35), thus eliminating the need of equation (35).

The last boundary condition is concerned with the compatible deformations of the wafer and anvil at their mating surface. An approximate relation which relates the average slope of the anvil to that of the wafer is given as

$$[(\omega)_{r=0} - (\omega)_{r=R_t}]_{\text{ANVIL}} = [|(\omega)_{r=0} - (\omega)_{r=R_t}|z = h]_{\text{WAFER}} \quad (37)$$

If the anvils are considered to be semi-infinite elastic bodies, the deflections due to a normal stress, continuously distributed

within a circular region, are given in reference [10] as

$$[(\omega)_{r=0}]_{\text{ANVIL}} = \frac{1-\nu}{G} \int_0^{R_t} \sigma_z dr$$

$$[(\omega)_{r=R_t}]_{\text{ANVIL}} = \frac{1-\nu}{GR_t} \int_0^{R_t} \sigma_z r dr \qquad (38)$$

A combination of equations (14), (24), (37), and (38) results, after lengthy computations, in the final required boundary condition equation. If a series solution had been used for the displacement function ψ, in lieu of the three terms shown in equation (12), it may have been possible to match deflections at each point of the wafer-anvil and wafer-containing ring interfaces, thus providing more appropriate boundary conditions. However, the boundary conditions stated in the foregoing are close approximations, and their use eliminates the drastic and unjustified increase in mathematical complexity associated with the addition of more terms to equation (12).

The equations (29), (32), (34), (36), and (38) represent five independent equations for the determination of the three displacement coefficients, a_1, a_2, a_3, the mid-meridian constraining pressure, P_c, and the wafer center line deflection, ∇. Once these quantities are known, the displacements, strains, stresses, and applied force can all be found by utilizing the appropriate equations. When each of the foregoing equations is expanded, the thought of obtaining an explicit equation for each of the unknowns is out of the question. The complexity of these equations provided the motivation for writing a computer program that would solve for the unknowns, using an interaction scheme. A further discussion of the computer programs and results are given later.

A portion of the motivation for using a displacement function in the solution of this problem relates to the ease in which existing solutions for wafer compression that apply for the case of more liberal assumptions can be verified from the more general treatment provided herein. For example, had the displacement coefficient a_2, in equation (12), been omitted (or set equal to zero), the resulting equations would define the stress state in a wafer that expands, without barreling, upon application of a compressive load. Similarly, it can be shown that if a_3 is the only nonvanishing displacement coefficient, the result corresponds to the compression of a wafer between perfectly lubricated, rigid anvils. These, and other aspects of the general compression of wafers, are discussed fully in reference [8].

Experimental

A complete description of the experimental facilities and procedure is given elsewhere (reference [8]) and will not be repeated in its entirety here. As defined previously, the wafer is a short circular cylinder, and has a diameter-to-height (D/H) ratio ranging from 3 to 13. The primary wafer material is annealed 303 stainless steel, and the secondary materials are 2S aluminum, 6061 aluminum, and Armco iron. The materials were purchased as bar stock, and all wafers of a particular material were taken with identical cuts from the same bar. Standard compression tests were conducted on specimens of each material to obtain the desired material constants. The compression specimens have a D/H ratio of 0.4 and are coated with molybdenum disulphide to minimize the end-effects. The material constants are determined by fitting equation (6) to the experimental stress-strain curves.

The radial constraint applied to the expanding wafer is attained through the utility of a containing ring assembly, which is composed of the following items:

1 **Wedges.** The purpose of the wedges is to transmit, in an elastic manner, the high-intensity restraining pressure existing at the external wafer surface, to a low-intensity pressure level at the larger inner surface of the steel containing ring. This intensification is inversely proportional to the radial position.

Since the wedges are not joined to one another, no hoop stresses are developed, and the wedges are in a state of compressive stress. The high compressive strengths available in Graph-Air metals suggested their use as the wedge material. By employing an ambient air quench from 1475 deg, and a further air quench to −11 deg with Dry Ice, the compressive elastic limit of the Graph-Air was raised to 400,000 psi. These precautions were taken to assure that the wafer is confined in an elastically deformable surrounding, consistent with the assumption employed in the analysis.

2 **Steel Containing Ring.** This ring serves as a radial support for the wedges and was designed to withstand an internal pressure of 50,000 psi. 4140 steel, heat-treated to a 190,000 psi yield strength, was used as the ring material. A slight interference fit between the steel containing ring and wedges was provided to maintain the assembly as an integral unit.

3 **Safety Ring.** As the name implies, the safety ring is constructed of a ductile material (303 stainless steel) and serves to restrain the motion of the internal parts in case a fracture should occur.

The anvil design is shown in Fig. 2 with the containing ring. The wafer makes actual contact with the anvil cones, which in turn are seated in a conical wedge assembly. The anvil wedges are supported by two press-fitted containing rings and an outer safety ring. The anvil cones were fabricated from Graph-Air and were designed in the conical shape to take advantage of the supporting stresses.

An assembly view of the wafer-containing ring system appears in Fig. 2. It should be noted that the wafer thickness is slightly greater than the corresponding thickness of the containing ring, which prevents the anvils from making contact with the ring. Three equally spaced rubber tabs are placed on the upper and lower sides of the containing ring to keep it centered until the expanding wafer makes contact. Two SR-4 foil-type strain gages have been mounted at diametrically opposed positions on the outer surface of the containing ring such that an average circumferential strain can be recorded as a function of the applied force. In conducting compression tests on confined wafers, the ram load was increased in even increments, and the circumferential strain, as read on the Baldwin indicator, was recorded at each increment. In the unconfined wafer tests, the mid-meridian wafer diameter was measured with micrometers and documented against the corresponding axial load. The loss of axial symmetry occurring with large (greater than 30 percent) radial deformations required that several diametral measurements be made, and the average recorded.

The lubricants used were molybdenum disulphide and iron oxide. According to reference [13], these lubricants have coefficients of friction of 0.04 and 0.71, respectively. These lubricating
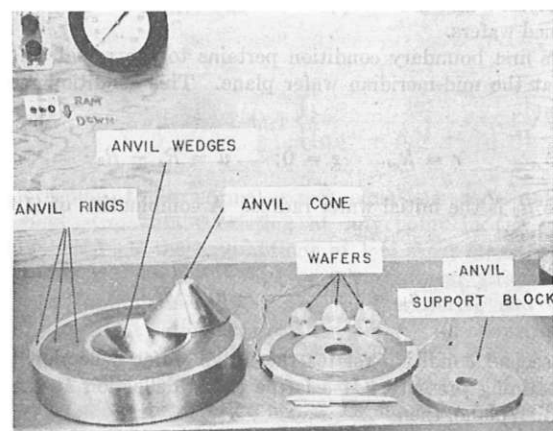

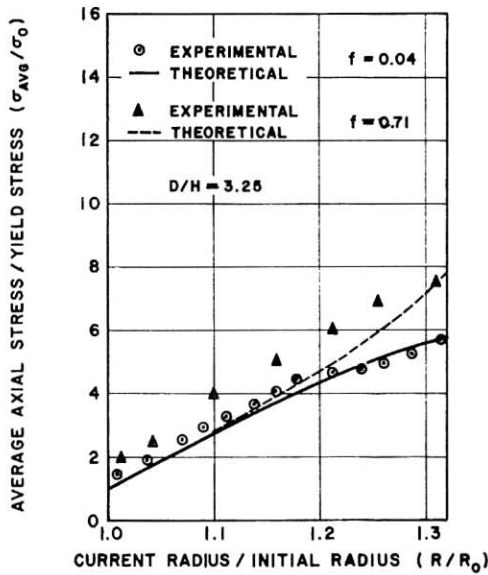**Fig. 2 Component parts of confined wafer compression system**

Fig. 3 Applied force displacement relation for an unconfined 303 stainless steel wafer

Fig. 4 Stress distribution for 303 stainless steel. Case 1-A

Fig. 5 Stress distribution for 303 stainless steel. Case 1-B.

powders were first mixed with an alcohol solution and then brush-coated on the wafer-anvil surfaces. Upon drying, a thin, uniform coat of lubricant was deposited on the desired surfaces.

The applied force-strain data taken from the confined wafer, and the applied force-radial deformation measurements acquired from the compression of unconfined wafers, have been documented in the various figures of the following section. This procedure permits a direct comparison between the experimental data and that which has been determined from the preceding analysis.

Results

The experimental and analytical applied force-displacement results achieved in the compression of an unconfined 303 stainless steel wafer are shown in Fig. 3. The ordinate of this, and subsequent force-displacement diagrams, have been nondimensionalized by dividing the applied force, equation (27), by the wafer surface area and the material yield strength σ_0. The abscissa has likewise been nondimensionalized by forming the ratio of current radius to initial radius. The predicted curve is in good agreement with the data for the low-friction lubricant (molybdenum disulphide), but the same comparison for the high-friction lubricant is not as favorable, except perhaps, at the approach of higher loads. This latter disagreement is to be expected since the analysis was predicated on the Hencky Deformation theory, which in turn requires that the surface shear stress be small. Since the applied force corresponds to the area under the axial normal stress curve, its agreement with the experimental data suggests strongly that the stress distributions are also valid.

The stress distributions occurring in a radial direction across the top and mid-meridian surfaces of a compressed, unconfined 303 stainless steel wafer are shown in Fig. 4. To aid in the identification of the type of compression test, a case number has been assigned to each of the stress distribution diagrams. The first character is a I or II, with the I meaning unconfined, and II represents a confined wafer. The second character is an A or B where A indicates that the anvil lubricant is molybdenum disulphide, and B represents iron oxide. Since the stresses are symmetrical about the wafer axis, the second half of the diagram is reserved for showing the results of an increased load. In Fig. 4, the stresses induced by the loads required to cause 16 percent and 32 percent increases in the initial radius are shown on the left and right sides, respectively. The axial stress σ_z and shearing stress τ_{rz} are obtained from equations (24) and (25), respectively, and the pressure P is found by taking the average of the normal
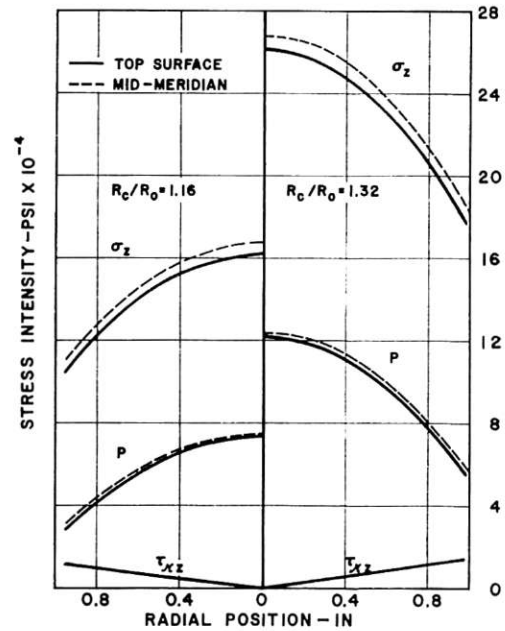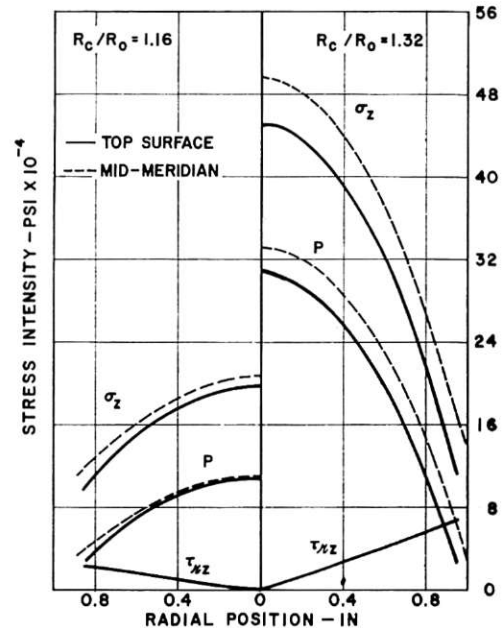
stresses, equations (22), (23), and (24). The computer programs used in finding the appropriate displacement coefficients, stresses, and applied forces are given in reference [8].

A comparison of Figs. 4 and 5 illustrates the influence of different anvil lubricants on the stress distribution. Molybdenum disulphide (coefficient of friction = 0.04) was used in Fig. 4, and iron oxide (coefficient of friction = 0.71) was the lubricant for Fig. 5. The higher surface friction retards the radial expansion and causes an intensification of the stresses at the wafer center. The shearing stress vanishes along the wafer axis and on the mid-meridian plane by virtue of symmetry. Both of these figures indicate that the axial variations are not significant for the unconfined wafer, especially in the low shear case. This latter case

also points out the discrepancy involved in assuming that the pressure in the wafer is the total force divided by wafer area, or what is equivalent, the average value of the normal axial stress σ_z.

The influence of wafer material properties has been examined from the results of compression tests on 6061 aluminum and Armco iron. Typical applied force-displacement, and stress distribution diagrams have been constructed in the manner described earlier, and are shown in the following figures. Wafers having two different D/H ratios were constructed from 6061 aluminum, and their applied force test results were superposed in Fig. 6 to show the apparent agreement with the analysis. This figure indicates that the wafer shape (D/H ratio) does not play a major role in the compression of unconfined wafers, within the range studied herein. Fig. 7 represents the corresponding stress and pressure distributions for 6061 aluminum, and it is noted that the stresses are still highest at the wafer center, and that the axial variations are small. The applied force-displacement and stress distribution results for Armco iron are not shown here; however, the conclusions are essentially the same as that stated for the aluminum wafers.
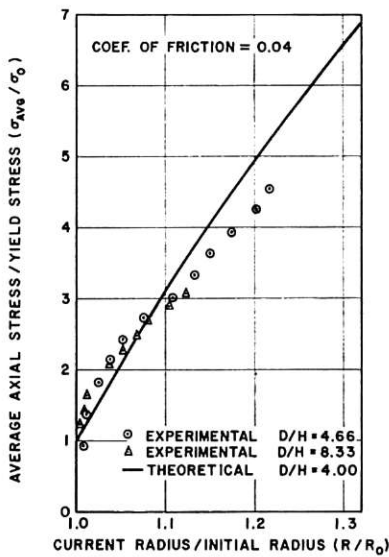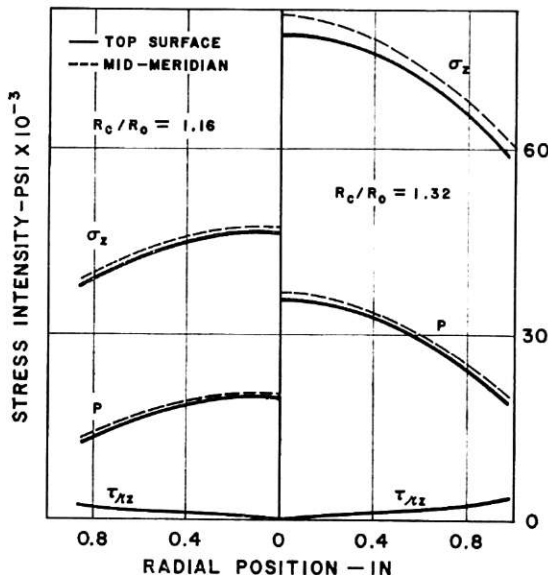
The tangential strain occurring at the mid-meridian surface of the containing ring has been documented against the applied force required for the compression of a confined 303 stainless steel wafer, and the results are shown with the analytical data in Fig. 8. The excellent agreement shown here is especially encouraging in view of the magnitude of the applied load (one million pounds). The experimental results do not pass through the origin since a certain minimum initial clearance must exist between the wafer and ring to provide for assembly. The analytical curve also starts above the origin since it was assumed that the wafer material is rigid until the onset of plastic straining. If the initial clearance and the elastic deformation of the wafer are the same, the two results would be compatible at the start. The stress distributions occurring across the top and mid-meridian surfaces of a confined 303 stainless steel wafer, subjected to a load corresponding to a 1.2 percent increase in initial radius, are shown in Fig. 9. Both sides of the diagram are employed to effectively illustrate the large stress gradients which occur in both the radial and axial directions of a confined wafer. The radial stress gradients are of the type encountered in the unconfined wafer; however, the axial gradients are appreciably greater, and this observation will be commented on later. Fig. 10 illustrates the stress gradients within the above wafer after the load has been increased until the mid-meridian wafer radius is 2.4 percent larger than its original value. These last two figures indicate that the radial gradients tend to level out with increase in load, and that the entire stress state approaches more closely to a hydrostatic condition.

In order to evaluate the effects of wafer shape (D/H ratio) on the stress distribution in confined wafers, two additional calculations were made with all parameters, except wafer shape, being the same as those utilized in Fig. 10. The new diameter-to-height ratios were 6.5 and 13, and the results of these last three computations have been combined to give a descriptive account of the influence of wafer shape on the profile of the axial normal stress distribution. Using the ratio of the axial stress at the wafer center to the average axial stress as the parameter for describing the stress profile, the curve appearing in Fig. 11 shows, for D/H in the range of 3 to 13, that the normal axial stress distribution across the wafer surface is maximum at the wafer center, and that the axial stress gradient in the radial direction becomes larger with increase in the wafer diameter-to-height ratio. The effect of neglecting the material strain hardening is to give values of the

Fig. 6 Applied force displacement relation for an unconfined 6061 aluminum wafer

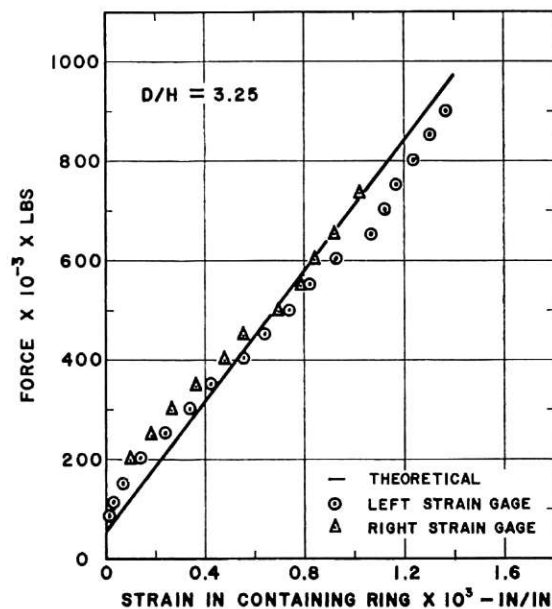Fig. 7 Stress distribution for 6061 aluminum. Case 1-A.

Fig. 8 Applied force strain relation for a confined 303 stainless steel wafer

computed applied force that are considerably less than that found in experiment. However, the extent of material strain hardening does not significantly affect the character of the stress distributions within the wafer.

One last item of interest is the description of the strain variations that are dictated by the analysis. Fig. 12 illustrates the strain distributions occurring in confined and unconfined wafers of 303 stainless steel. These strains are calculated from equa-

tions (15), (16), and (17) and are to be considered as companions for the stress distribution graphs shown in Figs. 4 and 9.

The agreement achieved between experimental data and the two-dimensional analysis is deemed good, and the resulting stress gradients are considered to be defensible in view of the manner in which they were found.
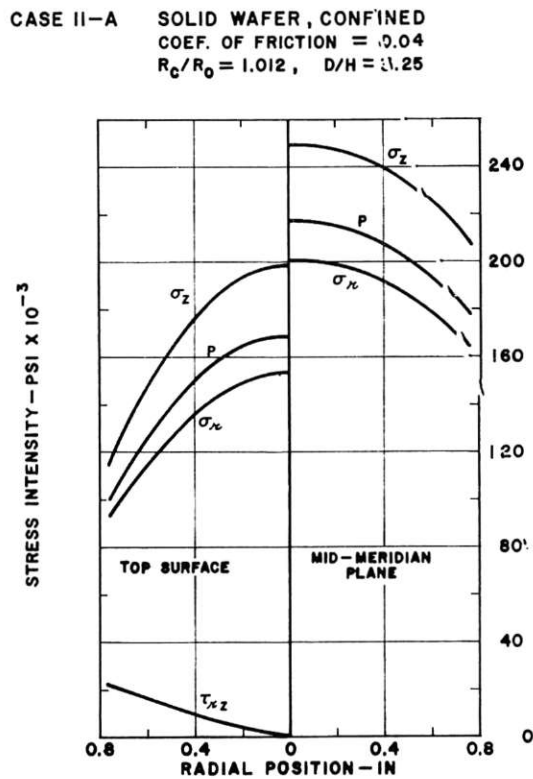
Fig. 9 Stress distribution for 303 stainless steel. Case II-A. $R_c/R_0 = 1.012$.
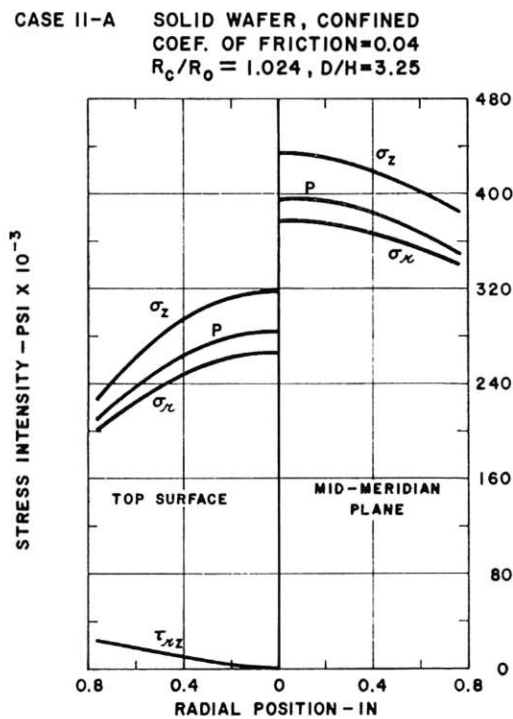
Fig. 10 Stress distribution for 303 stainless steel. Case II-A. $R_c/R_0 = 1.024$.
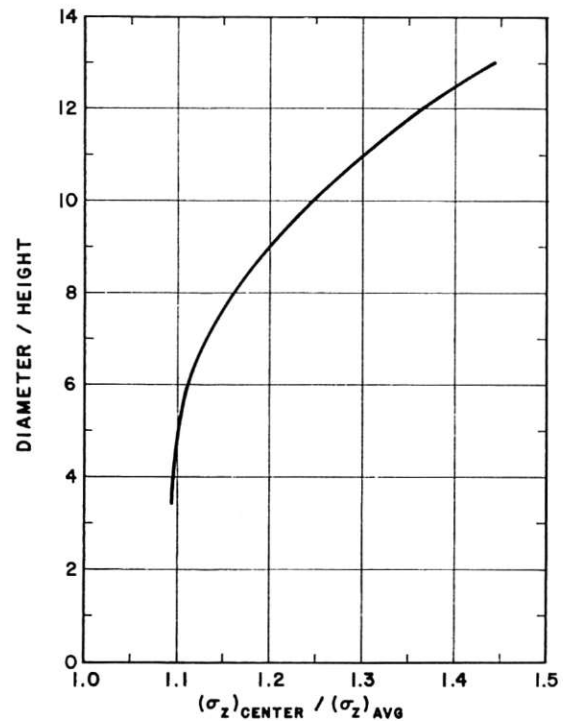
Fig. 11 Influence of wafer shape on axial stress gradient for 303 stainless steel
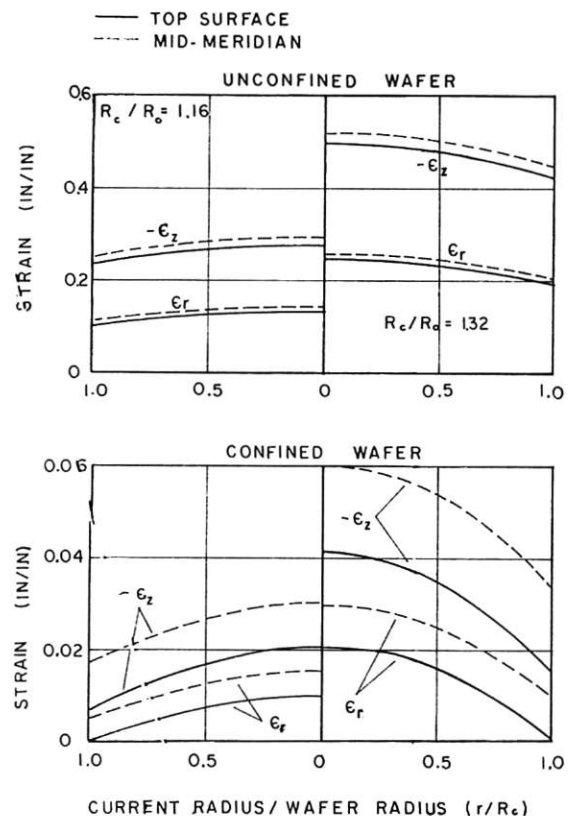
Fig. 12 Strain distribution

Summary and Conclusions

The method of solution used in the analysis of one and two-dimensional parametric variations in the compression of cylindrical wafers is considered to be valid and is adequately supported with numerous experimental data. The use of the displacement function has served to demonstrate the type of solution to be obtained with a retention of the appropriate terms. It also indicates the next term to be added if a more extensive analysis is to be performed. The solutions are limited to situations involving low shearing stresses at the anvil-wafer interface and are somewhat cumbersome to use. However, in view of the fact that the solutions embody the effects of material strain hardening, anvil deflection, surface shear, radial constraints, magnitude of load and strain, etc., they should be regarded as useful analytical tools for determining the stress and pressure gradients existing in Bridgman-type pressure cells (a term generally adapted for confined compression wafers). In the compression of unconfined, short cylinders, these solutions should also describe the "end effects" that are commonly excluded.

The stress distributions, for confined and unconfined wafers, all indicate that the stress, and pressure, is greatest at the wafer center and decreases with increase in radial position. This observation is consistent with the results reported in references [4], [7], and [14] and is in partial agreement with the conclusions of reference [6]. The admittance of a containing ring around the wafer enhances the prospect of obtaining pressures in the 5×10^5 psi range, especially at the wafer center. Evidence is presented, Figs. 9 and 10, which supports the argument that the stress state in a radially supported pressure cell approaches a hydrostatic condition with a sufficient increase in applied load. The containing ring need not remain elastic, nor should it act solely on the wafer, if the main purpose is to generate ultra-high pressures. The reason for doing such here is to obtain an experimental model that is more nearly compatible with the mathematical assumptions. The limited information obtained for high surface friction, iron oxide lubricant, indicates that the shearing stresses restrain the radial expansion of the wafer, in much the same manner as a containing ring, and serves to intensify the stress level at the wafer center and to increase the axial variations of pressure.

This paper entertains the effects of the variables pertinent to pressure cell constructions that have not previously been resolved. The method of solution permits a re-evaluation of the simpler analyses now available and lends itself to an extension to problems of more complexity. This work is an extension of results presented in reference [15], but is not terminal and will be pursued from different points of view until more elaborate and satisfactory results have been achieved.

References

1 J. W. Jackson and M. Waxman, "An Analysis of Pressure and Stress Distribution Under Rigid Bridgman-Type Anvils," High-Pressure Measurement Symposium, New York, Butterworths, 1963.

2 R. L. Carson, "Compression of a Viscoplastic Disk," ASME Paper No. 63—WA-98.

3 E. P. Unksov, An Engineering Theory of Plasticity, London, Butterworths, 1961.

4 L. N. G. Filon, et al., Photoelasticity, New York, Cambridge University Press, 1957.

5 H. Stromberg, et al., "Calibration of Bridgman Anvils, a Pressure Scale to 125 Kb," High-Pressure Measurement Symposium, New York, Butterworths, 1963.

6 R. Roy, et al., "Contribution to Calibration of High-Pressure Systems From. Studies in an Opposed-Anvil Apparatus," High-Pressure Measurement Symposium, New York, Butterworths, 1963.

7 J. E. Tydings and A. A. Giardini, "A Study of Stress Homogeneity in Cylindrical Cavities at High Pressures," High-Pressure Measurement Symposium, New York, Butterworths, 1963.

8 R. L. Davis and J. W. Jackson, "A Plastic Stress Analysis of Cylindrical Wafers Under Elastically Deformable Compression Plates," Complete report available from authors; University of Maryland, Mechanical Engineering Department Report 1965-1.

9 O. Hoffman and G. Sachs, Theory of Plasticity for Engineers, McGraw-Hill Book Co. Inc., New York, N. Y., 1953.

10 A. Nadai, Theory of Flow and Fracture of Solids, vol. 2, McGraw-Hill, New York, N. Y., 1963.

11 P. Ludwik, Elements der Technologischen Mechanik, Springer, Berlin.

12 P. B. Mellor and W. Johnson, Plasticity for Mechanical Engineers, D. Van Nostrand, New York, N. Y., 1962.

13 R. H. Wentorf, Jr., Modern Very High Pressure Techniques, Washington, Butterworths, 1962.

14 E. R. Lippincott and H. C. Duecker, "Distribution of Pressure in an Opposed-Anvil, High-Pressure Cell," Pressure Technology Session, ASME Winter Annual Meeting, New York, Paper No. 64—WA/PT-15.

15 J. W. Jackson and R. L. Davis, "An Analysis of the Stress Distribution Under Elastically Deformable Bridgman-Type Pressure Anvils," Pressure Technology Session, ASME Winter Annual Meeting, New York, ASME Paper No. 64—WA/PT-27.